



Deposited via The University of Leeds.

White Rose Research Online URL for this paper:

<https://eprints.whiterose.ac.uk/id/eprint/80811/>

Article:

Blanco, PH, Wu, C, Onwudili, JA et al. (2013) Characterization and evaluation of Ni/SiO catalysts for hydrogen production and tar reduction from catalytic steam pyrolysis-reforming of refuse derived fuel. *Applied Catalysis B: Environmental*, 134-13. 238 - 250. ISSN: 0926-3373

<https://doi.org/10.1016/j.apcatb.2013.01.016>

Reuse

See Attached

Takedown

If you consider content in White Rose Research Online to be in breach of UK law, please notify us by emailing eprints@whiterose.ac.uk including the URL of the record and the reason for the withdrawal request.

Characterization and evaluation of Ni/SiO₂ catalysts for hydrogen production and tar reduction from catalytic steam pyrolysis-reforming of RDF

Paula H. Blanco, Chunfei Wu, Jude A. Onwudili, Paul T. Williams*

Energy Research Institute, University of Leeds, Leeds, LS2 9JT, UK

(Tel: #44 1133432504; Email: p.t.williams@leeds.ac.uk)

Abstract: A series of Ni/SiO₂ catalysts have been prepared and investigated for their suitability for hydrogen production and tar reduction in a two-stage pyrolysis-reforming system, using refuse derived fuel (RDF) as the raw material. Experiments were conducted at a pyrolysis temperature of 600 °C, and a reforming temperature of 800 °C. The product gases were analysed by gas chromatography (GC) and the condensed fraction was collected and quantified using gas chromatography-mass spectrometry (GC-MS). The effects of the catalyst preparation method, nickel content and the addition of metal promoters (Ce, Mg, Al), were investigated. Catalysts were characterised using BET surface area analysis, temperature programmed oxidation (TPO), and scanning electron microscopy (SEM). The TPO and SEM analysis of the reacted catalysts showed that amorphous type carbons tended to be deposited over the Ni/SiO₂ catalysts prepared by impregnation, while filamentous type carbons were favoured with the sol-gel prepared catalysts. The influence of catalyst promoters (Ce, Mg, Al) added to the Ni/SiO₂ catalyst prepared by the sol-gel method was found not to be significant, as the H₂ production was not increased and the tar formation was not reduced with the metal-added catalyst. The highest H₂ concentration of 57.9 vol.% and lower tar amount produced of 0.24 mg_{tar}/g_{RDF}; were obtained using the 20 wt.% Ni/SiO₂ catalyst prepared by sol-gel. On the other hand a low catalytic activity for H₂ production and higher tar produced were found for the impregnated series of catalysts, which might be due to the smaller surface area, pore size and due to the formation of amorphous carbons on the catalyst surface. Alkenes and alcohol functional groups were mainly found in the analysed tar samples, with major concentrations of styrene, phenol, indene, cresols, naphthalene, fluorene, and phenanthrene.

Keywords: Tar; Nickel catalysts; Pyrolysis; Reforming; RDF; Syngas

1 Introduction

The search for new sustainable feedstocks to supply the projected increased world hydrogen demand is increasing [1]. The reforming of solid wastes has been regarded as a potential source for hydrogen production and the reforming of Refuse Derived Fuel (RDF), obtained from municipal solid waste (MSW), has attracted interest. RDF possess a heterogeneous composition with different fractions of inorganic and organic fractions containing materials such as paper, plastics, metals, etc., depending on its generation source [2, 3]. The thermal processing of RDF produces a high-valuable syngas rich in H₂ and CO, that can be further used in a variety of applications such as combustion in a turbine for heating and power generation [4], fuel cells and internal combustion engines [5]. Unfortunately the syngas produced from RDF also contains unacceptable levels of tar, which decreases the quality of the product gas. Additionally tar can condense at different process stages causing diverse operating problems such as blockages in pipelines, filters, turbines, and valve plugging. Tar can also promote corrosion in different equipment and as a result there is an increase in the costs of the process, and a decrease in the overall reforming yield [6, 7]. Therefore tar reduction or tar cracking is one of the major challenges for reforming implementation.

So far many definitions of tar have been made, however generally it is taken to mean a mixture of condensable hydrocarbons with a molecular weight larger than benzene (78 g mol⁻¹) [8-10], mixed with other oxygen-containing hydrocarbons, and polycyclic aromatic hydrocarbons (PAH) [7, 11]. A tar formation pathway based on temperature, was presented in our previous work [12].

The chemical reactions carried out during the tar formation process involve a complex mix of hydrocarbon decomposition and equilibrium reactions. A set of decomposition reactions, have been proposed by Simell et al [13], using toluene as a tar model compound; and include steam reforming, steam dealkylation, hydrocracking, hydrodealkylation, dry reforming, carbon formation, and an additional cracking reaction was added by Lind et al [14].

Nickel based catalysts have been extensively used for steam reforming processes to promote tar cracking during the reforming process as they enhance the steam-reforming reaction, and due to their strong ability for C-C bond rupture of some oxygenated hydrocarbons [15, 16]. Additionally Ni-based catalysts promote the reduction in the reforming temperature, and an increase in the hydrogen content of the syngas produced [17-19]. The influence of the preparation method over the catalysts properties has been previously reported in the literature [18, 20], also different oxide supports such as SiO₂ [18, 21] and

Al_2O_3 [15, 22] have been tested for their efficiency on tar reduction and catalyst properties. Ni/SiO₂ catalysts have been studied for methanol and ethanol reforming [18, 23], and for tar reforming [24] giving a good performance. SiO₂ was chosen as the support because it produces a higher metallic surface area and higher sintering resistance compared with other oxide supports [25]. Different promoters such as Ce, Al, and Mg have been added to different Ni-based catalysts in order to increase their catalytic activity and selectivity, to enhance the steam adsorption, and to reduce the carbon deposition over the catalyst surfaces [5, 26-28].

In this work a two-stage pyrolysis/reforming system was used to investigate the performance of a series of prepared Ni/SiO₂ catalysts, using RDF as the raw material. The catalysts were prepared by two different techniques in order to study the effect of the preparation method in relation to the catalyst characteristics; the effect of the Ni loading and the addition of metals to the catalysts were also examined. The prepared catalysts were compared in relation to their efficiency for hydrogen production and tar reduction.

2 Materials and Experimental

2.1 Materials

Municipal Solid Waste in the form of Refuse Derived Fuel (RDF) with a particle size of about 1.0 mm was used as the raw material in this work. The elemental and proximate analyses of the RDF has been reported in our previous work [12]; the samples contained 40 wt.% of carbon (C), 6 wt.% of hydrogen (H), 32 wt.% of oxygen (O), and 0.5 wt.% of nitrogen (N).

Nickel based catalysts, at different Ni loadings (5 wt.%, 10 wt.%, 20 wt.%, and 40 wt.%) were prepared by a sol-gel method, also three different metal supports (Al, Mg, and Ce) were added to the 20 wt.% Ni/SiO₂ sol-gel catalyst [18, 29]. Nickel nitrate hexahydrate ($\text{Ni}(\text{NO}_3)_2 \cdot 6\text{H}_2\text{O}$; Sigma-Aldrich), anhydrous citric acid (Alfa Aesar), deionised water, absolute ethanol (Sigma-Aldrich) and tetraethyl silicate (TEOS; $\text{Si}(\text{OC}_2\text{H}_5)_4$) (Sigma-Aldrich) were used as raw materials. The metals used for addition to the Ni/SiO₂ catalyst were derived from $\text{Ce}(\text{NO}_3)_3 \cdot 6\text{H}_2\text{O}$ (Aldrich), $\text{Al}(\text{NO}_3)_3 \cdot 9\text{H}_2\text{O}$ (Sigma-Aldrich), and $\text{Mg}(\text{NO}_3)_2 \cdot 6\text{H}_2\text{O}$ (Alfa Aesar); with a nickel loading of 20 wt.%. Different amounts of $\text{Ni}(\text{NO}_3)_2 \cdot 6\text{H}_2\text{O}$ (catalyst precursor), citric acid and metal support (if applicable) were dissolved into 200 ml of absolute ethanol, and stirred at 60 °C for 3 hours. A solution of different volumes of deionised water and 50 ml of absolute ethanol was added and stirred for another 30 minutes at 60 °C. Then the amount of TEOS was dropped into the solution to obtain the desired Ni:Si ratio. The solution was dried at 80 °C overnight, after drying the precursor was calcined at

500 °C for 4 hours in the presence of air. The catalysts prepared by the sol-gel method with 5, 10, 20 and 40 wt.% Ni loadings were assigned as 5Ni/SiO₂-A, 10Ni/SiO₂-A, 20Ni/SiO₂-A and 40Ni/SiO₂-A, respectively. In addition, metal added Ni/SiO₂ catalysts prepared by the sol-gel method were assigned as Mg-Ni/SiO₂-B, Al-Ni/SiO₂-B, and Ce-Ni/SiO₂-B, respectively.

Ni-based catalysts were also prepared by a wet impregnation method for comparison with the sol-gel method [18]. Different amounts of Ni(NO₃)₂·6H₂O (Sigma-Aldrich), were dissolved into 25 ml of deionised water and mixed with silicon (IV) oxide (amorphous SiO₂, 99.5% Alfa Aesar CAS 7631-86-9). The precursor was stirred at 100 °C for 30 minutes; dried overnight at 105 °C and calcined at 500 °C in an air atmosphere for 3 hours. The catalysts were designated as 5Ni/SiO₂-C, 10Ni/SiO₂-C, 20Ni/SiO₂-C, and 40Ni/SiO₂-C, for 5 wt.%, 10 wt.%, 20 wt.%, and 40 wt.% Ni loadings, respectively.

All the prepared catalysts were crushed and sieved to obtain finer particles with a size between 0.050 mm-0.180 mm. None of the prepared catalysts were reduced as during the process some of the produced gases such as H₂ and CO have the capability to reduce the catalyst itself [30].

2.2 Pyrolysis-reforming reactor system

The prepared catalysts were investigated for their influence over tar reduction and hydrogen production during the pyrolysis-reforming of refuse derived fuel (RDF), at a catalyst/RDF ratio of 0.5 g g⁻¹.

Pyrolysis-reforming of RDF was carried out using a two-stage fixed-bed reaction system in the presence of different Ni/SiO₂ catalysts. 2 grams of RDF were placed in a sample container and placed in the first pyrolysis stage. A bed of catalyst was placed in the second reforming stage. The experimental procedure consisted of the initial heating of the reforming stage up to 800 °C, followed by pyrolysis of RDF at a heating rate of 30 °C min⁻¹ to the final temperature of 600 °C. Steam was introduced at the top of the second stage, reforming reactor when the temperature of the first reactor reached around 230 °C; which was the thermal degradation temperature of the RDF [31]. The steam was mixed with the RDF pyrolysis gases, and then passed through the second catalytic stage with the aid of nitrogen as carrier gas (80 ml min⁻¹). Both pyrolysis and reforming temperatures were kept constant during all the experiments at 600 °C and 800 °C respectively; the electrical furnaces of each stage were thermally controlled separately. The steam was injected in the form of water, using a water

injection pump with a flow rate of 5 ml h^{-1} . The schematic diagram of the two stage reactor system used is presented on Figure 1.

The gaseous products exiting from the bottom of the reactor were passed through a series of condensers cooled by air and dry-ice; the condensed water and tars/oils were collected at the bottom of the condensers. The uncondensed gases were collected in a 10 L TedlarTM gas sample bag. The gases were collected for 20 minutes more after each experiment to ensure all of the produced gases were collected. The reproducibility and reliability of the experimental part were tested doing several repetitions of each experiment and were found to be satisfactory [12].

The collected gases were analysed by packed column gas chromatography to determine hydrocarbons ($\text{C}_2\text{-C}_4$) and permanent gases (H_2 , CO , N_2 , O_2 , CO_2). Hydrocarbons were analysed by a Varian CP-3380 gas chromatograph with a flame ionization detector (GC/FID) containing a column packed with 80-100 mesh Hysep; nitrogen was used as carrier gas. The permanent gases were analysed by a second Varian CP-3380 chromatograph provided with two packed columns, each one with a thermal conductivity detector (GC/TCD). The first column (used to separate hydrogen, carbon monoxide, nitrogen, and oxygen) was packed with a 60-80 mesh molecular sieve, and the second column (used to analyse carbon dioxide) was packed with 80-100 mesh; the carrier gas used was argon.

2.2.1 Tar analysis

The aqueous fraction condensed at the bottom of the condensers was collected using dichloromethane (DCM, analytical reagent grade, Fischer Scientific). The tar mixed with DCM, and the water fractions were physically separated. The water traces contained in the tar/oil mixed with DCM samples were extracted using a sodium sulphate bed (Na_2SO_4); the salt was previously dried for 2 hours at $140 \text{ }^\circ\text{C}$. The DCM contained in the samples was evaporated at around $30 \text{ }^\circ\text{C}$ using a Genevac Rocket Evaporation system, to obtain concentrated samples at the same volume. The tar composition was determined using a Varian CP-3800 gas chromatograph coupled with a Varian Saturn 2200 GC/MS/MS mass spectrometer. 2 micro litres of the tar solution in DCM were injected into the GC injector port at a temperature of $290 \text{ }^\circ\text{C}$; the oven programme temperature was $40 \text{ }^\circ\text{C}$ for 2 minutes, then ramped to $280 \text{ }^\circ\text{C}$ at $5 \text{ }^\circ\text{C min}^{-1}$ heating rate, and finally held at $280 \text{ }^\circ\text{C}$ for 10 minutes. The transfer temperature line was $280 \text{ }^\circ\text{C}$, manifold at $120 \text{ }^\circ\text{C}$ and the ion trap temperature was held at $200 \text{ }^\circ\text{C}$. A 3-point calibration curve was constructed by injecting standard solutions containing mixtures of phenols and polyaromatic hydrocarbons (PAHs). The standard

solutions were prepared from aliquots of pure compounds and diluted with DCM to final concentrations of 60ppm and 100ppm.

2.2.2 Catalyst characterization

A Quantachrome NOVA 2200e series apparatus was used to determine the BET surface area and porosities of the fresh Ni/SiO₂ catalysts. 90mg of each catalyst was degassed at 120 °C for 2 hours under nitrogen atmosphere before analysis. The N₂ adsorption and desorption isotherms were obtained at 77K. The surface area was calculated using the MultiPoint Brunauer, Emmett & Teller (BET) method, the micropore and mesoporous volumes were calculated using the Dubinin-Radushkevich (DR) method, and the total pore volume and pore diameter were obtained by the Barrett, Joyner & Halenda (BJH) method. The amount of N₂ adsorbed at relative pressures near unity corresponds to the total amount adsorbed for both micropores (generally filled at low relative pressures) and mesopores (filled by capillary condensation at relative pressures above 0.2); therefore the mesopore volume might be obtained by subtracting the micropore volume (obtained using the D-R equation), from the total amount adsorbed determined at P/P₀=0.95 in this case [32-34].

The used catalysts were analysed by temperature-programmed oxidation (TPO) using a Stanton-Redcroft thermogravimetric analyzer (TGA) to analyse the coked carbons deposited over the surface of reacted catalysts, the differential thermogravimetric (DTG) results were also obtained; around 20 mg of the used catalyst were placed in the TGA sample crucible, and heated in an air atmosphere at 15 °C min⁻¹ to a final temperature of 800 °C, with a dwell time of 10 minutes. A high-resolution scanning electron microscope (SEM, LEO 1530) was used to characterize and examine the carbon deposited on the reacted catalysts.

3 Results and Discussion

3.1 Characterization of Fresh Catalysts

The physical properties of the fresh prepared catalysts were compared according to the different preparation parameters, which included the preparation method, nickel content, and metal addition (Al, Mg, Ce).

3.1.1 BET Analysis of fresh catalysts

The N₂ adsorption-desorption isotherms of the fresh catalysts were determined at various relative pressures (P/P₀); Figure 2 shows the adsorption-desorption isotherms obtained for the calcined Ni/SiO₂ catalysts. For the sol-gel catalysts (Figure 2a), the 5Ni/SiO₂-A system

presented an isotherm of the Type I according to the IUPAC classification [35]. This isotherm shows no hysteresis loop and generally is given by microporous solids with relatively small external surface area. Also in this type of isotherm the limiting uptake is governed by the accessible micropore rather than by the internal surface area. From Table 1, the 5Ni/SiO₂-A catalyst reported a surface area around 600m² g⁻¹; whereas very low mesoporous volume (0.008cm³ g⁻¹) and total pore volume (0.034cm³ g⁻¹) were reported; which confirms the microporous properties of this 5Ni/SiO₂-A catalyst. The isotherm of the 10Ni/SiO₂-A catalyst seems to be a combination between the isotherms of Type I and Type IV (Figure 2a); additionally in this isotherm a hysteresis loop of the H2-Type was depicted into the multilayer region (around P/P₀=0.5), generally associated with very complex structures and interconnected pores with different shapes and sizes [36]. For the series of sol-gel catalysts, the higher surface area around 800m² g⁻¹ was reported for the 10Ni/SiO₂ catalyst (Table 1); however this catalyst also reported lower mesoporous volume and total pore volume values compared with catalysts with higher Ni loadings (20 and 40wt.%). Both 20Ni/SiO₂-A and 40Ni/SiO₂-A catalysts presented isotherms of the Type IV (Figure 2a), generally associated to well-defined mesoporous materials with fairly narrow pore size distribution [37]. Additionally from Figure 2a, two main stages in the adsorption-desorption isotherms might be identified for both 20Ni/SiO₂-A and 40Ni/SiO₂-A catalysts; the first one appears at low pressures indicating an adsorbate monolayer formation on the pore surface; then a second stage takes place related with the multilayer formation at higher pressures [38]. The upward deviation in the multilayer region corresponds to hysteresis of the H1-Type, characteristic of mesoporous solids having uniform pore structures [39, 40]; also the onset of the hysteresis loop indicates the beginning of the capillary condensation in the pores [38]. From Table 1 it is observed that relatively high mesoporous volumes around 0.6 and 0.5cm³ g⁻¹ were obtained from the DR calculation method for the 20 and 40wt.% Ni loadings respectively; it has been reported that mesoporous materials tend to have ordered pore structures with narrow pore size distribution, high surface area and large pore volumes [41]. In general, as the Ni loading of the prepared sol-gel catalysts was increased from 10wt.% up to 40wt.%, the total pore volume and mesoporous volume of the catalysts were increased (Table 1); additionally the hysteresis loop becomes more pronounced and moves slightly to higher pressures into the multilayer region (Figure 2a); this trend might be related with a higher amount of vapour adsorbed.. In Figure 2b, the isotherms for the catalysts prepared by impregnation method are presented; all of them belong to the isotherm Type III, which might

be indicative of weak interactions between adsorbent-adsorbate [36]; also no hysteresis loop was observed in any of the isotherms for this type of catalysts.

By comparing the isotherms of the catalysts with 20 wt.% Ni loading, prepared by sol-gel and impregnation methods respectively, the difference in the isotherm trends (Figure 2a, b) might be explained due to both the preparation method and the type of raw materials used. For the sol-gel catalysts the silica gel was formed from the reaction between TEOS in the presence of citric acid, which has been reported to provide mesoporous amorphous silica with high specific surface areas; whereas for the impregnated catalysts the silica source came directly from silicon (IV) oxide, which leads to a material with weak adsorbent-adsorbate interactions. Pina and collaborators reported that Ni/SiO₂ catalysts prepared by the impregnation method tend to present weak interactions with the substrate and a greater tendency to agglomeration [42]. The effect of the preparation method on the catalyst characteristics has been previously studied for ethanol and methanol reforming, reporting better characteristics and performance for sol-gel prepared catalysts [18, 23]. Tomiyama et al [20], also reported larger surface areas for Ni/SiO₂ catalysts prepared by sol-gel, compared with the same catalysts prepared by incipient wet impregnation; which is in accordance with the values reported in the present work. The Ni/SiO₂ sol-gel catalysts present a wide pore diameter distribution, especially at higher Ni loadings, leading to larger pore diameters. The pore diameter distribution for the catalysts prepared by sol-gel (Table 1), increased in a monotonic fashion from 3.77nm to 12.61nm as the Ni loading increased. Wu and Williams [18], also reported that the average pore size seemed to increase as the Ni loading increased from 10 up to 50 wt.% for Ni/SiO₂ catalysts prepared by sol-gel method.

In Figure 2c are presented the isotherms obtained from the sol-gel catalysts impregnated with different metals (Mg, Ce, Al). From Figure 2c it is observed that the isotherms presented a similar trend and all of them were identified from the Type IV, characteristic of mesoporous materials. Very similar BET surface area and pore diameter values around 550m² g⁻¹ and 5.6nm respectively were reported for both Mg and Al-Ni/SiO₂-B catalysts; whereas the Ce-Ni/SiO₂-B catalyst reported a surface area higher than 700m² g⁻¹ with 6.6nm of pore diameter (Table 1). This suggests that the addition of Ce has less influence on the surface area or pore size of the prepared catalysts; but a reduction in these two parameters can be noticed with the addition of Mg and Al. Also, the addition of the metals could lead to the modification of active sites on the metal surface or in changes of the geometric structure of the catalyst surface, as has been reported by Wang et al [43]. From Table 1 it is also observed that the mesoporous volumes of the metal-added Ni/SiO₂ catalysts, compared with the mesoporous

volume of the 20Ni/SiO₂-A catalyst were reduced. A reduction in the mesopore volume has been previously reported by Ding and Yan during the addition of oxide promoters to Ni/Al₂O₃ catalysts [44]; they suggested that the oxide promoters, MgO and CeO₂, were concentrated on the outer layer of the support, and the nickel metal was dispersed in the support pores; as a result a reduction in mesopore volume might be promoted.

3.2 RDF pyrolysis/reforming using Ni/SiO₂ catalysts

The gas composition and gas yields are presented on Table 2. The gas composition of the gases derived from the pyrolysis-reforming of RDF was analysed and reported on a N₂ free basis. From Table 2, the results of gas composition using the Ni/SiO₂ catalysts prepared by the sol-gel method (A series), showed that the H₂ concentration of the produced gases increased as the Ni loading was increased, however with the 40Ni/SiO₂-A catalyst, the hydrogen concentration decreased slightly. The hydrogen production showed a similar trend with the changes of gas concentrations with the increase of the Ni loading for the A series catalyst; the highest hydrogen production was obtained for the 20Ni/SiO₂-A catalyst (26.5 mmol H₂ g⁻¹ RDF) (Table 2). CO₂ concentration was increased and the methane (CH₄) and light hydrocarbon (C₂-C₄) concentrations were considerably reduced as the Ni loading was increased.

With the increase of Ni loading, more catalytic sites were expected to be presented in the catalyst system, and contribute to a higher degree of hydrocarbon cracking or steam reforming reactions; thus hydrocarbon gases were seen to be reduced. Therefore, more gas production was obtained from the cracked hydrocarbons when the catalyst was changed from 5Ni/SiO₂-A to 40Ni/SiO₂. However, a saturation point of Ni loading may be reached when 40 wt.% of Ni was loaded in the Ni/SiO₂ catalyst. Since the H₂ concentration was not increased for the 40Ni/SiO₂-A compared with the 20Ni/SiO₂ catalyst (Table 2). It is interesting to find that the change of pore volume of the catalyst was similar to the change of H₂ production for the A-series catalyst. For example, highest mesoporous volume was obtained for the 20Ni/SiO₂-A catalyst (0.602 cm³ g⁻¹), while the highest H₂ production was produced for the same catalyst during the RDF pyrolysis-reforming process (Table 2). It is suggested that more gaseous products derived from the first-stage pyrolysis could enter into the pores and contact with catalytic Ni sites, when higher mesoporous volume was presented. In this work, catalytic Ni particles were incorporated inside the SiO₂ instead of at the surface of the SiO₂; therefore, accessibility of Ni catalytic sites will be important for hydrogen production. In addition, the increase of H₂ and CO₂ concentrations and the decrease of CO concentration with the

increase of Ni loading; this might be due to the promotion of water gas shift reaction due to the exothermic reaction. Similar results has been reported [45]. Furthermore, the increase of H₂/CO ratio from 1.44 to 3.41 (Table 2) also indicated that the water gas shift reaction was promoted with the increase of Ni loading for the A series catalyst during RDF pyrolysis-reforming process.

Three different metals were added to the 20Ni/SiO₂-A catalyst with the aim to improve the performance of this catalyst. For example Zapata and collaborators [46], added Ce to Ni/SiO₂ catalysts in order to promote methane reforming and the stability of the catalysts. Also Choudhary et al [28], added Mg to different supported Ni-catalysts to enhance the steam adsorption capability, to stabilize the Ni and to prevent catalyst sintering. From Table 2, it can be noted that similar CO₂ concentrations of ~22 vol.%, were obtained using Mg, Ce and Al added Ni/SiO₂-B catalysts. Regarding the H₂ concentration, 54 vol.% was obtained for Ce and Mg-Ni/SiO₂-B catalysts, while a H₂ concentration of 50 vol.% was obtained using the Al-Ni/SiO₂-B catalyst. The addition of Ce and Mg into Ni/SiO₂-B resulted in similar CH₄ concentration of 2.6 vol.%, while using the Al-Ni/SiO₂-B catalyst a CH₄ concentration of 5.3 vol.% was obtained. From the catalysts properties presented in Table 1, it was expected that Mg and Al addition to the Ni/SiO₂-B catalysts would produce similar gas composition, as both catalysts showed similar properties of surface area and pore volume. However, Al added Ni/SiO₂-B catalyst showed a much lower H₂ concentration and gas yield compared with the Mg- Ni/SiO₂-B catalyst (Table 2). Therefore, the catalytic performance in terms of hydrogen production and gas yield were also significantly influenced by the type of metals added into the base Ni/SiO₂ catalyst. From Table, Ce added Ni/SiO₂-B catalyst also showed a higher H₂ concentration and gas yield compared with the Al-Ni/SiO₂-B catalyst. Ce and Mg have been reported to promote methane steam reforming [46], to enhance the catalytic activity [47], and water-gas shift reactions [5]; while probably only a minor promotion could be obtained using Al.

[5, 27, 49, 50]. The addition of MgO as a promoter to different Ni-based catalysts can lead to a H₂ yield of 40% stoichiometric, during the steam reforming of bio-oil [5], whereas CH₄ conversions higher than 90% can be attained [28, 51]. The addition of the CeO promoter was also studied during the autothermal reforming of methane and partial oxidation of methane to syngas, leading to a CH₄ conversion up to 100% and attaining a H₂/CO maximum of 3.5 using Ni/Ce₃₀Al₇₀O₈ catalyst [26]. Slight differences in the gas yield can also be attributed to changes in the steam water injected during each experiment.

The influence of the preparation method on the performance of the Ni/SiO₂ catalysts during RDF pyrolysis-reforming was studied. The C series correspond to the impregnation prepared type of catalysts with different Ni loadings (Table 2). From Table 2, the highest hydrogen concentration was obtained using the 40Ni/SiO₂-C catalyst; the 10Ni/SiO₂-C and 20Ni/SiO₂-C catalysts reported a H₂ concentration of ~40 vol.%, and for the 5Ni/SiO₂-C catalysts the H₂ concentration was 36 vol.%. The CH₄ and C₂-C₄ concentrations were found to be reduced for all the impregnated catalysts, when the Ni loading was increased. However, compared with the A-series catalysts prepared by the sol-gel method, the C series catalysts showed lower yield of gas and H₂ concentration. The poor performance of Ni/SiO₂ catalyst prepared by impregnation in terms of hydrogen production might be ascribed to the low surface area and pore volume (Table 1). Better performance in relation to hydrogen production has also been reported for the sol-gel prepared catalyst compared with the impregnated catalyst by Wu and Williams during the steam reforming of ethanol [18]; also Goncalves et al [23], reported a better performance for Ni/SiO₂ sol-gel catalysts during the CO₂ reforming of CH₄ when compared with Ni/SiO₂ catalysts prepared by impregnation.

3.3 Tar analysis

3.3.1 GC-MS analysis of collected tar

A quantitative analysis to determine the tar composition of the tars derived from the pyrolysis-catalytic reforming of RDF was carried out using GC/MS/MS. The retention times of the peaks, the compounds assigned and their concentration expressed as $\mu\text{g}_{\text{compound}}/\text{g}_{\text{RDF}}$, are presented in Table 3. The results shown that the major compounds in terms of concentration ($\mu\text{g}_{\text{comp}}/\text{g}_{\text{RDF}}$), for most of the analysed samples were: styrene, phenol, indene, *p*-cresol, *m*-cresol, naphthalene, fluorene, and phenanthrene. In our previous work [12], a qualitative GC-MS analysis was carried out on tar samples derived from the pyrolysis/reforming of RDF using Ni/Al₂O₃ catalysts; the most common identified compounds in the analysed samples were: naphthalene, biphenyl, fluorene, phenanthrene, methylnaphthalene, catechols and alcohols. It can be noted that compounds such as naphthalene, fluorene and phenanthrene were also detected in the results presented here. In the present work, a quantitative analysis is presented, giving detailed information on the distribution of compounds in the tars. Some of the compounds identified here have been previously reported by others for the pyrolysis of RDF [52] and for biomass reforming using a secondary tar cleaning system [14].

In Table 3, the results show that the tar concentration was reduced from 1.66 to 0.24 $\text{mg}_{\text{tar}}/\text{g}_{\text{RDF}}$ as the nickel loading was increased for the sol-gel catalysts (series A). It can be noted that the tar concentration for the 20 and 40 wt.% Ni for the Ni/SiO₂-A catalysts is quite similar at 0.25 $\text{mg}_{\text{tar}}/\text{g}_{\text{RDF}}$, thus no major reduction was attained despite the increase in the Ni loading from 20 to 40 wt.% of the Ni/SiO₂ prepared by the sol-gel method. The tar reduction in relation to the Ni loading was increased from 5 up to 20 wt.% for the Ni/SiO₂-A catalyst might be related to the mesoporous volume of the catalysts (Table 1), as the mesoporous volume was increased with the increase of Ni loading. However, with further increase of Ni loading to 40 wt.%, the mesoporous volume was reduced from 0.602 to 0.492 $\text{cm}^3 \text{g}^{-1}$ (Table 1), resulting in an increase of the tar concentration (Table 3). In addition, the influence of Ni loading for the A series catalyst on the tar reduction corresponded with the influences on hydrogen and gas production (Table 2). Since, the hydrogen and gas yields were increased while tar content was reduced with the increase of Ni loading from 5 to 20 wt.%.

It was expected that the tar formation would be reduced by adding the metals Al, Mg, or Ce to the sol-gel catalyst, due to the enhancement of the catalytic activity by promoting cracking reactions, as reported previously during the partial oxidation of methane [53, 54]. Among the three promoters added to the 20Ni/SiO₂ catalyst, the highest activity in terms of tar reduction was shown by the Mg-Ni/SiO₂ catalyst with a tar content of 0.25 $\text{mg}_{\text{tar}}/\text{g}_{\text{RDF}}$ (Table 3); whereas Al and Ce-Ni/SiO₂ catalysts reported about twice that value. The addition of metal promoters such as CeO₂ to Ni based catalysts has been previously reported to promote tar removal during the biomass reforming process [55, 56], with positive effects compared with conventional Ni-based catalysts. For example Kimura et al [55], found that using CeO₂ as promoter of the Ni/Al₂O₃ catalyst, tar and coke might be converted to CO, H₂ and methane during the biomass steam reforming of biomass, thus reducing the tar and coke yields. The addition of MgO as metal promoter to Ni/SiO₂ catalysts has been also reported to improve coke resistance and to reduce sintering of Ni particles; hence the catalytic activity of the catalyst was improved [50]. However in this work neither the tar yield, was reduced (Table 3) nor hydrogen production was improved (Table 2) by adding Mg, Al or Ce as metal promoters to the sol-gel Ni based catalyst.

In the case of the catalysts prepared by impregnation, the tar amount was reduced from 1.67 up to 0.60 $\text{mg}_{\text{tar}}/\text{g}_{\text{RDF}}$ when the Ni loading was increased from 5 to 20 wt.%, but increased to 0.98 $\text{mg}_{\text{tar}}/\text{g}_{\text{RDF}}$ using the higher nickel content (40 wt% Ni) for the 40Ni/SiO₂-C catalyst. This might be related to the sintering of Ni particles due to the high nickel loading, and resulted in the lower catalytic activity. Mark and Maier [57] have reported that an

increase in the metal content could lead to a decrease in the metal dispersion of the catalyst. Therefore, it is suggested that the 40 wt.% of Ni loading on the Ni/SiO₂ catalyst prepared by the impregnation method was too high for hydrogen production from pyrolysis/reforming of RDF. Furthermore, the physical properties of this catalyst were not improved as the Ni loading was increased for this catalyst (Table 1), even more; the surface area of the 40Ni/SiO₂-C catalyst was reduced probably due to the high Ni loading used.

A classification of tar compounds has been previously presented in the literature by different authors [58-61]. This classification is based on the number of aromatic rings of the different compounds found in tar samples from different sources. Based on this classification, the identified compounds in the analysed samples were grouped and are presented in Table 4. The tar Class 1 is referred to as GC-undetectable compounds, for this reason is not included in this classification. The Class 2 corresponds mainly to heterocyclic compounds; compounds with 1 aromatic ring were grouped in Class 3; light polyaromatic compounds in Class 4, and tar Class 5 includes heavy polyaromatic compounds. Once the identified compounds were grouped, the concentration of the different tar Classes for the tars produced using the Ni/SiO₂ catalysts was obtained; the results are presented in Figure 3.

From Figure 3 it can be noted that for all the analysed samples the major tar contribution came from tar Class 2; these tars are sometimes referred to as primary tars and are known to contain mainly oxygenated compounds with aromatic and aliphatic structures [6]. Among the compounds grouped in tar Class 2, the major contribution came from the compound phenol for all the analysed samples. For the sol-gel catalysts (A series), a clear reduction in the concentration of phenol was attained as the Ni loading was increased (Table 3). In general the tar Class 2 concentration was reduced as the Ni loading was increased for the sol-gel catalysts (Figure 3). This reduction can be related to the pore diameter of the sol-gel catalysts (Table 1) as the pore diameter was increased as the Ni loading was increased, and also with the promotion of cracking of the heterocyclic aromatic compounds.

The phenol concentration (Table 3) varied with the content of Mg, Ce, and Al in the Ni/SiO₂-B metal promoted catalysts. The highest phenol concentration was obtained for the Ce-Ni/SiO₂-B catalyst, and the lowest concentration was attained using the Mg-Ni/SiO₂-B catalyst. Comparing the phenol concentration obtained using the 20Ni/SiO₂-A catalyst with the that obtained using the Mg-Ni/SiO₂-B catalyst (Table 3), a lower concentration was attained using the Mg promoter; this might be due to the presence of Mg reducing the carbon deposition and promoting a low sintering of Ni particles [5]. From Figure 3, the higher concentration of the tar Class 2, was obtained using the Ce and Al Ni/SiO₂-B catalysts,

whereas a remarkable reduction was attained using Mg as the metal promoter. This difference might be attributed to the long-term stability of the catalyst due to the addition of Mg metal [50], and also to the low sintering of Ni particles and high coke resistance reported previously by Wang and Lu [50].

A reduction in phenol concentration was also observed for the series of Ni/SiO₂-C catalysts prepared by the impregnation method (Table 3), as the Ni loading was increased; however the high 40 wt% Ni loading of the 40Ni/SiO₂-C catalyst generated the highest concentration of phenol compared with other Ni-loading catalysts; this can be related to the reduction in the surface area of the 40Ni/SiO₂-C catalyst (Table 1). From Figure 3, a reduction in concentration of tar Class 2 can be observed with increased Ni loading for the A series catalyst. However, tar Class 2 concentration was increased when the Ni loading was increased to 40 wt.% for the C series catalyst.

From Figure 3 it can be noted that the tar Class 3 corresponding to single ring aromatic compounds, was reduced as the Ni loading was increased for the sol-gel series of catalysts (A). A similar concentration of 0.1 mg_{tar-Class3}/g_{RDF} for the tar Class 3 was obtained using both 20 and 40Ni/SiO₂-A catalysts; this observation was consistent with changes of gas and hydrogen productions for the two catalysts (Table 2). For the addition of metal promoters (series B) the concentration of tar Class 3 was 0.04 mg_{tar-Class3}/g_{RDF} for both Ce and Al Ni/SiO₂-B catalysts, whereas a lower concentration of 0.02 mg_{tar-Class3}/g_{RDF} was obtained using the Mg-Ni/SiO₂-B catalyst. This reduction might be related to the nature of the metal that might be promoting more of the cracking of single ring aromatic compounds. For example, it has been reported that the addition of Mg might stabilize the Ni crystallite [54], thus enhancing the catalytic activity of the catalyst. For the catalysts prepared by the impregnation method, the lowest concentration of the tar Class 3 was attained using the 5Ni/SiO₂-C catalyst; while somewhat similar concentrations were reported using the 10, 20 and 40 Ni/SiO₂-C catalysts.

In this work, naphthalene has been included in the tar Class 4, which contributed significantly to the concentration of tar in the analysed samples (Figure 3). Naphthalene has been reported as a major compound in tar samples from the pyrolysis and/or reforming process [24, 62]. For example Abu El-Rub et al [63], used naphthalene and phenol as tar model compounds to measure tar reduction during the reforming process, using different catalyst types. Devi and collaborators [64], used naphthalene as a tar model compound, with olivine as the catalyst in order to improve the naphthalene conversion. Considering this, the reduction of naphthalene can be used as a measure of the efficiency of the prepared catalysts.

According to the concentrations reported in the Table 3, for the series of sol-gel catalysts (series A), a reduction in the naphthalene concentration was observed as the Ni loading was increased; however a considerable increase was noted using the 40Ni/SiO₂-A catalyst. A similar increase in the concentration of other compounds such as styrene, indene, phenanthrene, and fluoranthene; was also observed using the 40Ni/SiO₂-A catalyst which indicates that the reduction of these major compounds is not as effective as using the 20Ni/SiO₂-A catalyst. This might be due to the lower surface area and mesoporous volume obtained for the 40Ni/SiO₂-A catalyst (Table 1). By using the metal promoters Ce, Mg, and Al (series B), different concentrations of naphthalene were obtained with a better conversion using both Mg and Al Ni/SiO₂-B catalysts. However, the general concentrations of tar Class 4 using these metal-promoted catalysts were similar at 0.06 mg_{tar-Class4}/g_{RDF}, which was slightly higher compared with the 0.02 mg_{tar-Class4}/g_{RDF} concentration obtained using the 20Ni/SiO₂-A catalyst. For the series of impregnated catalysts a reduction of naphthalene was observed for the 10Ni/SiO₂-C catalyst (Table 3); but it is noted that using the 5Ni/SiO₂-C catalyst the lowest naphthalene concentration was attained. This effect can also be observed for other low molecular weight compounds such as styrene, and indene, but for higher molecular compounds such as fluorene, phenanthrene and fluoranthene, higher concentrations were obtained using the 5Ni/SiO₂-C catalyst. The total concentration of tar Class 4 was reduced as the Ni loading was increased for the impregnated catalysts; the lowest concentration attained was 0.15 mg_{tar-Class4}/g_{RDF}, using the 40Ni/SiO₂-C catalyst (Figure 3).

Fluoranthene, pyrene and 1,3,5-triphenylbenzene were identified and included in tar Class 5; the concentration of these compounds for all the samples was very low with a maximum tar concentration of 0.06 mg_{tar-Class5}/g_{RDF} using the 5Ni/SiO₂-A catalyst (Figure 3). A total conversion of tar Class 5 was attained using the Al-Ni/SiO₂-B catalyst, while very low concentrations of around 0.01 mg_{tar}/g_{RDF} were obtained using 20Ni/SiO₂-A, 40Ni/SiO₂-A, Mg-Ni/SiO₂-B, and 20-Ni/SiO₂-C catalysts (Figure 3). This suggests that the conversion of higher molecular weight compounds (>200 g mol⁻¹) included in Class 5, can be attained using Ni loadings from 20 wt.%, but also the influence of the preparation method should be considered, as for the 40-Ni/SiO₂-C catalyst a higher concentration of the tar Class 5 was attained (Figure 3).

In terms of tar reduction (Table 3), the best performance was obtained using the 20-Ni/SiO₂-A, 40-Ni/SiO₂-A, and Mg-Ni/SiO₂-B catalysts, resulting in tar concentrations lower than 0.3 mg_{tar}/g_{RDF}. The highest styrene, indene, and naphthalene conversions were obtained using the 20Ni/SiO₂-A catalyst, while the best phenol and fluorene conversions were

obtained using the 40-Ni/SiO₂-A catalyst. The highest fluoranthene and phenanthrene conversions were attained using the Al-Ni/SiO₂-B and 40-Ni/SiO₂-C catalysts respectively.

The catalysts that presented a better performance regarding general tar reduction were also found to have better performance in terms of hydrogen production as shown in Table 3 and Table 2, respectively. In general, the conversion of hydrocarbons during the reforming process might be attributed to steam cracking and CO₂ reforming reactions; the decrease in hydrocarbons are associated with an increase in hydrogen with a more effective catalyst [45].

3.4 Characterisation of coked catalysts

The reacted catalysts were analysed with TGA and SEM, in order to characterize the carbon deposited over the catalysts surfaces.

3.4.1 Thermogravimetric analysis (TGA)

The deposition of coke over the reacted catalysts was investigated by using thermogravimetric analysis (TGA). Temperature programmed oxidation curves (TGA-TPO), and their derivative curves (DTG-TPO) are shown in Figure 4a-c. According to the literature [18, 30, 65], at least three different stages can be identified with the thermogravimetric curves, when coked catalysts are analysed. The first stage involves a mass decrease due to water vaporization, identified from 0-100 °C [15]. The second stage corresponds to the Ni phase oxidation shown at around 350 °C, and finally carbon combustion after 400 °C [18]. Additionally two different types of carbon can be formed over the catalysts surface, amorphous and filamentous carbon. The amorphous carbon oxidation is suggested to initiate at around 500 °C, while the filamentous carbon oxidation can be observed at around 600 °C [30, 66].

The curves presented in Figure 4a, correspond to the sol-gel reacted catalysts with different Ni loadings. For the 5Ni/SiO₂-A catalyst the DTG-TPO curve is almost a straight line compared with the TPO results from the reacted 10, 20 and 40 wt.% Ni/SiO₂-A catalysts; this may be due to the low Ni loading and also due to the small amount of carbon deposition over the reacted 5Ni/SiO₂-A catalyst. For the 5, 10 and 20 wt.% Ni/SiO₂-A catalysts, a weight decrease can be noticed in the TGA-TPO curve before 100 °C, whereas in the DTG-TPO curve the respective peaks can be observed at the same temperature; this is due to water vaporization present in the catalysts. The DTG-TPO curves of the 10, 20 and 40 wt.% Ni/SiO₂-A catalysts (Figure 4a), show a weight increase at around 350 °C; that might be related to Ni oxidation as the higher peak corresponds to the 40-Ni/SiO₂-A catalyst.

Oxidation of filamentous carbon was suggested to start to be formed around 600 °C [18], in Figure 4a at least two peaks can be identified around 600 °C from 10Ni/SiO₂-A, and 20Ni/SiO₂-A catalysts, which might suggest the deposition of filamentous carbon on to the catalysts after pyrolysis-reforming of RDF. The coke deposition seems to be increased when the Ni loading was increased from 5 to 20 wt.% for the Ni/SiO₂-A catalysts prepared by the sol-gel method (Figure 4a). In addition, gas and hydrogen production was also increased with the increase of the Ni loading (Table 2). It is suggested that the carbons were produced through cracking of hydrocarbons and tars for the gas and hydrogen production. However, coke deposition was reduced using the 40Ni/SiO₂-A catalyst (Figure 4a) which might be due to the promotion of coke-steam reactions.

In Figure 4b, a comparison of the TPO analysis of the Mg, Ce, and Al Ni/SiO₂-B metal-added catalysts is presented. Initially a decrease in both the TGA and DTG curves can be observed, this weight reduction is due to moisture loss; after that three clear peaks related to a weight increase are observed in the DTG-TPO curves, related to metal oxidation. The trend for the three reacted catalysts is similar; however two peaks from the Mg and Ce Ni/SiO₂-B catalysts appear at around 400 °C (DTG-TPO), while the Al-Ni/SiO₂-B reacted catalyst peak appear around 600 °C. This difference can be related to the nature of the promoter added; Wang and Lu [43], have previously reported that the addition of metal oxides might influence the activity of the supported metal catalyst and also the coke formation on the catalyst surface. For example they showed that the addition of alkaline-earth metal promoters such as Mg to Ni/Al₂O₃ catalysts could significantly reduce coke formation on the catalyst surface during the CO₂ reforming of methane. Probably due to this, the reacted Mg-Ni/SiO₂-B catalyst has a smaller oxidation peak compared with the other metal promoters. As two different peaks can be observed in the DTG-TPO curves (Figure 4b), it might be suggested that different types of carbon were deposited over these catalysts, probably amorphous carbon was formed on the Ce and Mg-Ni/SiO₂-B catalysts, whereas filamentous carbon could be found in the Al-Ni/SiO₂-B reacted catalyst.

Figure 4c shows the TGA-TPO and DTG-TPO results for the series of catalysts prepared by the impregnation method. From Figure 4c it can be noted that the curves increased in a monotonic trend as the Ni loading was increased. For all the DTG-TPO curves a major peak appears between 400 °C and 500 °C, which can be due to the oxidation of nickel. An increase trend of this main peak can be observed as the Ni loading increased on the impregnated catalysts. The TGA-TPO curves of the reacted Ni/SiO₂-C catalysts shown that the weight

ratio was increased when the Ni loading increased from 5 to 40 wt.%, probably due to more Ni particles were available for oxidation with higher Ni loading.

Comparing the TPO analysis for the 20Ni/SiO₂-A and 20Ni/SiO₂-C catalysts prepared by the sol-gel and impregnation methods respectively (Figure 4a, and 4c), the carbon combustion appears immediately after 400 °C for the impregnated catalyst (Figure 4c), whereas for the sol-gel catalyst appears after 600 °C (Figure 4a). It is suggested that for reacted impregnated catalysts, amorphous carbons were formed during the pyrolysis/reforming of RDF; while for the reacted sol-gel catalysts the deposition of filamentous carbon is observed.

3.4.2 Scanning Electron Microscopy (SEM)

High-resolution scanning electron microscopy (SEM LEO 1530) was used to characterize the carbon deposited on the reacted Ni/SiO₂ catalysts; the images of the surface morphology are presented in Figure 5.

From Figure 5 it was noted that for the sol-gel catalysts (5, 10, 20, 40 Ni/SiO₂-A), filamentous carbon was deposited over the surface. The observation of filamentous carbons was consistent with the results obtained from the TPO analysis (Figure 4), where an oxidation peak of filamentous carbon was found at around 650 °C. By adding the metal promoters, it was observed that different amounts of filamentous and probably amorphous carbon were deposited over the surface of the Mg-Ni/SiO₂-B, Al-Ni/SiO₂-B, and Ce-Ni/SiO₂-B catalysts. The images of the Mg-Ni/SiO₂-B and Ce-Ni/SiO₂-B catalysts were more similar, whereas the SEM image of the Al-Ni/SiO₂ catalyst differs regarding the type of coke deposited. From Figure 4b it can be observed that the DTG-TPO curve of the Al-Ni/SiO₂-B catalyst, showed its main peak at higher temperatures compared with the other two reacted catalysts; this might suggest the formation of two different carbon types. Finally the images of the reacted surface of the impregnated catalysts presented very little coke deposition mainly from amorphous type carbon. In the image of the 10Ni/SiO₂-C catalyst (Figure 5), some filamentous carbon could be observed. From the TPO and SEM results (Figure 4 and Figure 5), filamentous carbons might tend to be deposited over the reacted Ni/SiO₂ sol-gel catalysts, whilst amorphous carbons are deposited over the reacted catalysts prepared by the impregnation method. Also two different types of carbon were deposited over the sol-gel catalysts prepared using metals as promoters, despite both types of filamentous and amorphous carbon were found in these catalysts, the amount of each one influenced the

DTG-TPO curves giving a better idea about the trend of carbon deposited over the surface of each reacted catalyst.

4 Conclusions

In this paper, a series of Ni/SiO₂ catalysts were prepared, characterised and investigated for their efficiency in relation to hydrogen production and tar reduction during the pyrolysis/reforming of RDF in a two-stage reaction system. The results suggest that:

- 1) Ni/SiO₂ catalysts prepared by the sol-gel method were shown to be effective catalysts for the production of hydrogen and tar reduction. The best performance was attained using the 20 wt.% Ni/SiO₂ catalyst prepared by sol-gel.
- 2) Catalysts prepared by the sol-gel method showed higher catalytic activity related to hydrogen and gas production compared with the catalyst prepared by impregnation.
- 3) Unexpectedly there was no significant positive influence on hydrogen production or tar reduction with the addition Ce, Mg or Al to the 20 wt.% Ni/SiO₂ sol-gel catalyst; as the catalysts characteristics, produced gas composition (hydrogen production), and tar reduction were not improved.
- 4) The tar from the pyrolysis/reforming of RDF was found to contain mainly styrene, phenol, indene, cresols, naphthalene, fluorene, and phenanthrene, from the alkene and alcohol functional groups.
- 5) Filamentous carbon was more likely to be deposited over the reacted sol-gel catalysts, while amorphous carbon was found over the reacted surfaces of impregnated catalysts. Both types of carbon were deposited over the promoted catalysts depending on the metal nature, and its interaction with the Ni phase.

Acknowledgements

The authors would like to thank the National Council of Science and Technology of Mexico (Conacyt) for a scholarship of one of us: PHB. We would also like to thank the UK Engineering and Physical Sciences Research Council (EPSRC) for support for this work under research grant number EP/G036608/1.

References

- [1] C. Wu, P.T. Williams, Effects of Gasification Temperature and Catalyst Ratio on Hydrogen Production from Catalytic Steam Pyrolysis-Gasification of Polypropylene, *Energy Fuel*, 22 (2008) 4125-4132.
- [2] H.J. Ollila, A. Moilanen, M.S. Tiainen, R.S. Laitinen, SEM-EDS characterization of inorganic material in refuse-derived fuels, *Fuel*, 85 (2006) 2586-2592.
- [3] J. Fellner, P. Aschenbrenner, O. Cencic, H. Rechberger, Determination of the biogenic and fossil organic matter content of refuse-derived fuels based on elementary analyses, *Fuel*, 90 (2011) 3164-3171.
- [4] P.R. Ramage, R. Agrawal, *The Hydrogen Economy: Opportunities, Costs, Barriers and R&D Needs*, Washington, DC, 2004.
- [5] L.a. Garcia, R. French, S. Czernik, E. Chornet, Catalytic steam reforming of bio-oils for the production of hydrogen: effects of catalyst composition, *Applied Catalysis A: General*, 201 (2000) 225-239.
- [6] P. Morf, Secondary Reactions of Tar during Thermochemical Biomass Conversion, in, *Swiss Federal Institute of Technology Zurich, Zurich, 2001*, pp. 177.
- [7] C. Li, K. Suzuki, Tar property, analysis, reforming mechanism and model for biomass gasification--An overview, *Renewable and Sustainable Energy Reviews*, 13 (2009) 594-604.
- [8] K. Maniatis, A.A.C.M. Beenackers, Tar Protocols. IEA Bioenergy Gasification Task, *Biomass and Bioenergy*, 18 (2000) 1-4.
- [9] L. Devi, K.J. Ptasiński, F.J.J.G. Janssen, A review of the primary measures for tar elimination in biomass gasification processes, *Biomass and Bioenergy*, 24 (2003) 125-140.
- [10] J.P.A. Neeft, H.A.M. Knoef, P. Onaji, S.E.C. Nederland, B.B.T. Group, *Behaviour of Tar in Biomass Gasification Systems: Tar Related Problems and Their Solutions*, Novem, 1999.
- [11] E. Larsen, Egsgaard, H., Pedersen, K., Zielke, U., Brandt, P., Tar compounds in condensates from different types of gasifiers, in: S. Kyritsis (Ed.) *1st World Conference on Biomass for Energy and Industry*, James & James (Science Publishers) Ltd, Sevilla, Spain, 2000, pp. 2137.
- [12] P.H. Blanco, C. Wu, J.A. Onwudili, P.T. Williams, Characterization of Tar from the Pyrolysis/Gasification of Refuse Derived Fuel: Influence of Process Parameters and Catalysis, *Energy Fuel*, 26 (2012) 2107-2115.
- [13] P.A. Simell, Hepola, J. O., Krause, A. O., Effects of gasification gas components on tar ammonia decomposition over hot gas cleanup catalysts, *Fuel*, 76 (1997) 1117-1127.
- [14] F. Lind, M. Seemann, H. Thunman, Continuous Catalytic Tar Reforming of Biomass Derived Raw Gas with Simultaneous Catalyst Regeneration, *Industrial & Engineering Chemistry Research*, 50 (2011) 11553-11562.
- [15] A.J. Akande, R.O. Idem, A.K. Dalai, Synthesis, characterization and performance evaluation of Ni/Al₂O₃ catalysts for reforming of crude ethanol for hydrogen production, *Applied Catalysis A: General*, 287 (2005) 159-175.
- [16] M. Ni, D.Y.C. Leung, M.K.H. Leung, A review on reforming bio-ethanol for hydrogen production, *International Journal of Hydrogen Energy*, 32 (2007) 3238-3247.
- [17] C. Li, D. Hirabayashi, K. Suzuki, Development of new nickel based catalyst for biomass tar steam reforming producing H₂-rich syngas, *Fuel Processing Technology*, 90 (2009) 790-796.
- [18] C.F. Wu, P.T. Williams, A Novel Nano-Ni/SiO₂ Catalyst for Hydrogen Production from Steam Reforming of Ethanol, *Environmental Science & Technology*, 44 (2010) 5993-5998.
- [19] M.P. Aznar, M.A. Caballero, J. Gil, J.A. Martín, J. Corella, Commercial Steam Reforming Catalysts To Improve Biomass Gasification with Steam-Oxygen Mixtures. 2. Catalytic Tar Removal, *Industrial & Engineering Chemistry Research*, 37 (1998) 2668-2680.
- [20] S. Tomiyama, R. Takahashi, S. Sato, T. Sodesawa, S. Yoshida, Preparation of Ni/SiO₂ catalyst with high thermal stability for CO₂-reforming of CH₄, *Applied Catalysis A: General*, 241 (2003) 349-361.

- [21] N.J. Tang, W. Zhong, W. Liu, H.Y. Jiang, X.L. Wu, Y.W. Du, Synthesis and complex permeability of Ni/SiO₂ nanocomposite, *Nanotechnology*, 15 (2004) 1756-1758.
- [22] L.I. Darvell, K. Heiskanen, J.M. Jones, A.B. Ross, P. Simell, A. Williams, An investigation of alumina-supported catalysts for the selective catalytic oxidation of ammonia in biomass gasification, *Catalysis Today*, 81 (2003) 681-692.
- [23] G. Goncalves, Lenzi, M. K., Santos, O. A. A., Jorge, L. M. M., Preparation and characterization of nickel based catalysts on silica, alumina and titania obtained by sol-gel method, *Journal of Non-Crystalline Solids*, 352 (2006) 3697-3704.
- [24] J. Srinakruang, K. Sato, T. Vitidsant, K. Fujimoto, Highly efficient sulfur and coking resistance catalysts for tar gasification with steam, *Fuel*, 85 (2006) 2419-2426.
- [25] A. Gil, A. Díaz, L.M. Gandía, M. Montes, Influence of the preparation method and the nature of the support on the stability of nickel catalysts, *Applied Catalysis A: General*, 109 (1994) 167-179.
- [26] X. Cai, X. Dong, W. Lin, Effect of CeO₂ on the catalytic performance of Ni/Al₂O₃ for autothermal reforming of methane, *Journal of Natural Gas Chemistry*, 17 (2008) 98-102.
- [27] Q. Miao, G. Xiong, S. Sheng, W. Cui, L. Xu, X. Guo, Partial oxidation of methane to syngas over nickel-based catalysts modified by alkali metal oxide and rare earth metal oxide, *Applied Catalysis A: General*, 154 (1997) 17-27.
- [28] V.R. Choudhary, B.S. Uphade, A.S. Mamman, Oxidative Conversion of Methane to Syngas over Nickel Supported on Commercial Low Surface Area Porous Catalyst Carriers Precoated with Alkaline and Rare Earth Oxides, *Journal of Catalysis*, 172 (1997) 281-293.
- [29] C. Wu, P.T. Williams, Hydrogen production from steam reforming of ethanol with nano-Ni/SiO₂ catalysts prepared at different Ni to citric acid ratios using a sol-gel method, *Applied Catalysis B: Environmental*, 102 (2011) 251-259.
- [30] C. Wu, P.T. Williams, Hydrogen production by steam gasification of polypropylene with various nickel catalysts, *Applied Catalysis B: Environmental*, 87 (2009) 152-161.
- [31] W.K. Buah, A.M. Cunliffe, P.T. Williams, Characterization of Products from the Pyrolysis of Municipal Solid Waste, *Process Safety and Environmental Protection*, 85 (2007) 450-457.
- [32] C.T. Hsieh, H.S. Teng, Influence of mesopore volume and adsorbate size on adsorption capacities of activated carbons in aqueous solutions, *Carbon*, 38 (2000) 863-869.
- [33] H.S. Teng, C.T. Hsieh, Influence of surface characteristics on liquid-phase adsorption of phenol by activated carbons prepared from bituminous coal, *Industrial & Engineering Chemistry Research*, 37 (1998) 3618-3624.
- [34] F. Rodríguez-Reinoso, M. Molina-Sabio, M.T. González, The use of steam and CO₂ as activating agents in the preparation of activated carbons, *Carbon*, 33 (1995) 15-23.
- [35] K.S.W. Sing, D.H. Everett, R.A.W. Haul, L. Moscou, R.A. Pierotti, J. Rouquerol, T. Siemieniewska, Reporting Physisorption Data for Gas Solid Systems with Special Reference to the Determination of Surface-Area and Porosity (Recommendations 1984), *Pure Appl Chem*, 57 (1985) 603-619.
- [36] F. Rouquerol, J. Rouquerol, K.S.W. Sing, *Adsorption by Powders and Porous Solids*, Academic Press, London, 1999.
- [37] P. Kim, Y. Kim, H. Kim, I.K. Song, J. Yi, Synthesis and characterization of mesoporous alumina with nickel incorporated for use in the partial oxidation of methane into synthesis gas, *Applied Catalysis A: General*, 272 (2004) 157-166.
- [38] S. Naumov, Hysteresis Phenomena in Mesoporous Materials, in: *Physics and Earth Sciences*, University of Leipzig, Leipzig, 2009.
- [39] C.T. Chiou, *Partition and Adsorption of Organic Contaminants in Environmental Systems*, John Wiley & Sons, Inc., Hoboken, New Jersey, 2002.
- [40] K.S.W. Sing, *Adsorption Methods for Surface Area Determination*, in: N.G. Stanley-Wood, Lines, R. W. (Ed.) *Particle Size Analysis*, Royal Society of Chemistry, Cambridge, UK, 1992, pp. 13-32.
- [41] P. Kim, Y. Kim, T. Kang, I. Song, J. Yi, Preparation of nickel-mesoporous materials and their application to the hydrodechlorination of chlorinated organic compounds, *Catalysis Surveys from Asia*, 11 (2007) 49-58.

- [42] G. Pina, C. Louis, M.A. Keane, Nickel particle size effects in catalytic hydrogenation and hydrodechlorination: phenolic transformations over nickel/silica, *Phys Chem Chem Phys*, 5 (2003) 1924-1931.
- [43] S. Wang, G.Q. Lu, Effects of promoters on catalytic activity and carbon deposition of Ni/ γ -Al₂O₃ catalysts in CO₂ reforming of CH₄, *Journal of Chemical Technology & Biotechnology*, 75 (2000) 589-595.
- [44] R.G. Ding, Z.F. Yan, Adsorption properties studies of the nickel catalysts for carbon dioxide reforming of methane., *Abstr Pap Am Chem S*, 223 (2002) U563-U563.
- [45] F. Pinto, R.N. André, C. Franco, H. Lopes, I. Gulyurtlu, I. Cabrita, Co-gasification of coal and wastes in a pilot-scale installation 1: Effect of catalysts in syngas treatment to achieve tar abatement, *Fuel*, 88 (2009) 2392-2402.
- [46] B. Zapata, M.A. Valenzuela, J. Palacios, E. Torres-Garcia, Effect of Ca, Ce or K oxide addition on the activity of Ni/SiO₂ catalysts for the methane decomposition reaction, *International Journal of Hydrogen Energy*, 35 (2010) 12091-12097.
- [47] J. Li, J. Liu, S. Liao, R. Yan, Hydrogen-rich gas production by air-steam gasification of rice husk using supported nano-NiO/ γ -Al₂O₃ catalyst, *International Journal of Hydrogen Energy*, 35 (2010) 7399-7404.
- [48] Z.L. Zhang, V.A. Tsipouriari, A.M. Efstathiou, X.E. Verykios, Reforming of Methane with Carbon Dioxide to Synthesis Gas over Supported Rhodium Catalysts: I. Effects of Support and Metal Crystallite Size on Reaction Activity and Deactivation Characteristics, *Journal of Catalysis*, 158 (1996) 51-63.
- [49] A.S.A. Al-Fatesh, A.H. Fakeeha, A.E. Abasaeed, Effects of promoters on methane dry reforming over Ni catalyst on a mixed (α -Al₂O₃+TiO₂-P25) support, *International Journal of the Physical Sciences*, 6 (2011) 8083-8092.
- [50] S. Wang, G.Q.M. Lu, CO₂ reforming of methane on Ni catalysts: Effects of the support phase and preparation technique, *Applied Catalysis B: Environmental*, 16 (1998) 269-277.
- [51] V.R. Choudhary, B.S. Uphade, A.S. Mamman, Large enhancement in methane-to-syngas conversion activity of supported Ni catalysts due to precoating of catalyst supports with MgO, CaO or rare-earth oxide, *Catalysis Letters*, 32 (1995) 387-390.
- [52] P.T. Williams, S. Besler, Polycyclic aromatic hydrocarbons in waste derived pyrolytic oils, *Journal of Analytical and Applied Pyrolysis*, 30 (1994) 17-33.
- [53] M. Li, X. Wang, S. Li, S. Wang, X. Ma, Hydrogen production from ethanol steam reforming over nickel based catalyst derived from Ni/Mg/Al hydrotalcite-like compounds, *International Journal of Hydrogen Energy*, 35 (2010) 6699-6708.
- [54] S.M. Richardson, M.R. Gray, Enhancement of Residue Hydroprocessing Catalysts by Doping with Alkali Metals, *Energ Fuel*, 11 (1997) 1119-1126.
- [55] T. Kimura, T. Miyazawa, J. Nishikawa, S. Kado, K. Okumura, T. Miyao, S. Naito, K. Kunimori, K. Tomishige, Development of Ni catalysts for tar removal by steam gasification of biomass, *Applied Catalysis B: Environmental*, 68 (2006) 160-170.
- [56] K. Tomishige, T. Kimura, J. Nishikawa, T. Miyazawa, K. Kummori, Promoting effect of the interaction between Ni and CeO₂ on steam gasification of biomass, *Catal Commun*, 8 (2007) 1074-1079.
- [57] M.F. Mark, W.F. Maier, CO₂-Reforming of Methane on Supported Rh and Ir Catalysts, *Journal of Catalysis*, 164 (1996) 122-130.
- [58] L. Devi, K.J. Ptasinski, F.J.J.G. Janssen, S.V.B. van Paasen, P.C.A. Bergman, J.H.A. Kiel, Catalytic decomposition of biomass tars: use of dolomite and untreated olivine, *Renewable Energy*, 30 (2005) 565-587.
- [59] J. Han, H. Kim, The reduction and control technology of tar during biomass gasification/pyrolysis: An overview, *Renewable and Sustainable Energy Reviews*, 12 (2008) 397-416.
- [60] C. Brage, Q. Yu, K. Sjöström, Characteristics of evolution of tar from wood pyrolysis in a fixed-bed reactor, *Fuel*, 75 (1996) 213-219.

- [61] A. Ponzio, S. Kalisz, W. Blasiak, Effect of operating conditions on tar and gas composition in high temperature air/steam gasification (HTAG) of plastic containing waste, *Fuel Processing Technology*, 87 (2006) 223-233.
- [62] K. Sato, K. Fujimoto, Development of new nickel based catalyst for tar reforming with superior resistance to sulfur poisoning and coking in biomass gasification, *Catal Commun*, 8 (2007) 1697-1701.
- [63] Z. Abu El-Rub, E.A. Bramer, G. Brem, Experimental comparison of biomass chars with other catalysts for tar reduction, *Fuel*, 87 (2008) 2243-2252.
- [64] L. Devi, K.J. Ptasinski, F.J.J.G. Janssen, Pretreated olivine as tar removal catalyst for biomass gasifiers: investigation using naphthalene as model biomass tar, *Fuel Processing Technology*, 86 (2005) 707-730.
- [65] S. Wang, G.Q. Lu, Role of CeO₂ in Ni/CeO₂-Al₂O₃ catalysts for carbon dioxide reforming of methane, *Applied Catalysis B: Environmental*, 19 (1998) 267-277.
- [66] C. Wu, P.T. Williams, Investigation of coke formation on Ni-Mg-Al catalyst for hydrogen production from the catalytic steam pyrolysis-gasification of polypropylene, *Applied Catalysis B: Environmental*, 96 (2010) 198-207.

Table 1. Surface properties of prepared sol-gel Ni/SiO₂ catalysts

Catalyst	Ni content (wt%)	Surface area ¹ (m ² g ⁻¹)	Micropore volume ² (cm ³ g ⁻¹)	Mesoporous volume ² (cm ³ g ⁻¹)	Total pore volume ³ (cm ³ g ⁻¹)	Pore diameter ³ (nm)
5Ni/SiO ₂ -A	5	595.40	0.322	0.008	0.034	3.776
10Ni/SiO ₂ -A	10	836.90	0.398	0.231	0.315	3.820
20Ni/SiO ₂ -A	20	756.40	0.389	0.602	0.884	6.608
40Ni/SiO ₂ -A	40	481.56	0.260	0.492	0.755	12.612
Mg-Ni/SiO ₂ -B	20	554.40	0.281	0.400	0.583	5.660
Al-Ni/SiO ₂ -B	20	552.60	0.281	0.410	0.587	5.654
Ce-Ni/SiO ₂ -B	20	717.90	0.389	0.524	0.771	6.606
5Ni/SiO ₂ -C	5	6.89	0.003	0.010	0.029	3.172
10Ni/SiO ₂ -C	10	6.39	0.003	0.009	0.025	3.796
20Ni/SiO ₂ -C	20	9.70	0.003	0.010	0.019	3.374
40Ni/SiO ₂ -C	40	6.29	0.003	0.010	0.026	3.764

¹ MultiPoint Brunauer, Emmett & Teller (BET) Method

² Dubinin-Radushkevich (DR) Method

³ Barrett, Joyner & Halenda (BJH) Method

Table 2. Gas yield and gas composition from pyrolysis/reforming of RDF

Catalyst	Gas composition (Vol.%, N ₂ free)					Gas Yield (wt.%)	Hydrogen production (mmol H ₂ g ⁻¹ RDF)	<i>H₂/CO Ratio</i>	Mass Balance (wt.%)
	CO	H ₂	CO ₂	CH ₄	C ₂ -C ₄				
5Ni/SiO ₂ -A	28.6	41.2	15.4	8.8	6.1	45.7	10.2	1.44	94.8
10Ni/SiO ₂ -A	24.1	47.4	16.5	8.1	3.8	58.6	16.0	1.97	98.0
20Ni/SiO ₂ -A	18.4	57.9	20.7	2.2	0.8	68.7	26.5	3.15	91.6
40Ni/SiO ₂ -A	16.5	56.2	25.6	1.4	0.4	72.6	23.7	3.41	98.7
Ce-Ni/SiO ₂ -B	19.0	53.6	24.1	2.6	0.7	64.9	20.0	2.83	98.1
Mg-Ni/SiO ₂ -B	20.1	54.3	22.4	2.6	0.6	58.6	18.9	2.70	98.5
Al-Ni/SiO ₂ -B	21.6	49.6	22.0	5.3	1.5	46.4	12.9	2.30	94.2
5Ni/SiO ₂ -C	27.6	35.6	22.3	9.7	4.8	39.9	7.0	1.29	93.9
10Ni/SiO ₂ -C	29.2	37.7	20.5	8.8	3.8	46.8	9.2	1.29	94.6
20Ni/SiO ₂ -C	21.7	40.6	26.6	7.2	3.9	51.9	10.2	1.88	99.0
40Ni/SiO ₂ -C	22.3	44.1	25.8	5.7	2.1	55.4	12	1.98	98.6

Table 3. Identified compounds by GC-MS analysis

RT (min)	Assigned Peak	MW (g mol ⁻¹)	5Ni/SiO ₂ - A	10Ni/SiO ₂ - A	20Ni/SiO ₂ - A	40Ni/SiO ₂ - A	Ce- Ni/SiO ₂ - B	Mg- Ni/SiO ₂ - B	Al- Ni/SiO ₂ - B	5Ni/SiO ₂ - C	10Ni/SiO ₂ - C	20Ni/SiO ₂ - C	40Ni/SiO ₂ - C
7.84	Furfural	96	—	3.44	1.52	0.51	1.17	0.29	2.00	12.65	5.05	3.73	7.14
7.81	Cyclopentanone	84	—	7.44	1.45	0.47	1.18	0.00	2.08	13.39	3.63	3.66	7.02
8.67	Ethylbenzene	106	4.78	0.21	—	1.20	0.57	0.22	1.10	—	1.25	1.13	4.05
9.02	<i>p</i> -Xylene	106	—	0.95	3.06	1.79	8.53	2.47	4.96	0.44	4.09	5.36	7.10
9.02	<i>m</i> -Xylene	106	12.89	0.96	3.18	1.78	8.31	2.40	4.81	0.59	4.07	5.30	6.90
9.86	Styrene	104	115.99	21.26	1.41	8.51	31.09	15.16	27.07	3.13	44.25	43.77	43.04
9.89	<i>o</i> -Xylene	106	2.83	—	—	—	2.36	1.64	2.65	—	—	—	—
13.36	Phenol	94	867.12	407.95	183.82	129.98	404.50	160.29	377.08	1019.04	419.71	292.79	606.86
13.78	Para-methylstyrene	118	7.07	—	—	—	—	—	—	1.27	—	—	—
14.97	Indane	118	2.32	1.40	—	0.24	0.18	0.25	0.22	0.25	1.01	0.92	0.54
15.35	Indene	116	182.18	95.32	1.23	8.27	11.00	21.50	9.05	5.89	55.95	68.09	28.16
15.69	<i>o</i> -Cresol	108	27.37	15.77	2.72	2.51	4.99	1.28	7.91	—	28.37	10.66	12.46
16.14	Acetophenone	120	1.24	5.10	0.99	1.24	—	0.43	1.04	3.70	—	1.16	1.71
16.47	<i>p</i> -Cresol	108	71.52	—	5.58	6.50	15.56	5.00	15.07	105.59	81.00	27.77	35.19
16.48	<i>m</i> -Cresol	108	34.25	5.04	5.34	6.03	11.03	4.61	18.11	72.57	63.96	24.74	32.75
17.38	2-Methylbenzofuran	132	6.55	—	—	0.75	—	0.43	0.30	—	—	1.55	1.49
18.29	2-Ethylphenol	122	1.47	—	—	—	—	—	—	2.24	1.83	—	2.47
18.66	2,4-Dimethylphenol	122	4.58	1.23	—	1.10	—	—	1.33	—	5.58	—	—
19.32	4-Ethylphenol	122	4.67	2.39	—	—	—	—	1.51	—	5.76	—	—
19.32	3-Ethylphenol	122	5.07	2.66	—	1.33	—	—	1.58	—	6.30	—	—
19.32	2,6-Dimethylphenol	122	5.23	2.72	—	1.47	—	—	1.66	—	6.47	—	—
19.93	Naphthalene	128	70.44	35.22	4.11	38.99	17.12	10.30	10.64	35.16	123.66	46.62	42.38
20.93	4-Isopropylphenol	136	—	—	—	—	—	—	—	—	—	—	2.48
23.16	2-Methylnaphthalene	142	17.18	16.15	1.62	3.33	2.65	2.26	3.23	17.17	24.60	7.95	9.10
25.08	Biphenyl	154	19.05	20.92	2.06	1.66	2.84	2.86	3.49	42.46	45.47	9.16	18.22
25.32	2-ethylnaphthalene	156	1.81	0.99	—	1.08	0.78	—	0.74	2.66	1.97	2.04	—
25.32	1-ethylnaphthalene	156	—	0.75	—	0.50	0.36	—	0.37	1.51	1.83	—	—
25.54	2,6-dimethyl naphthalene	156	2.06	1.06	—	—	0.65	—	0.69	3.69	2.77	1.86	3.36
26.16	1,4-dimethylnaphthalene	156	—	—	1.21	0.77	0.63	—	—	3.30	—	—	—

RT (min)	Assigned Peak	MW (g mol ⁻¹)	5Ni/SiO ₂ - A	10Ni/SiO ₂ - A	20Ni/SiO ₂ - A	40Ni/SiO ₂ - A	Ce- Ni/SiO ₂ - B	Mg- Ni/SiO ₂ - B	Al- Ni/SiO ₂ - B	5Ni/SiO ₂ - C	10Ni/SiO ₂ - C	20Ni/SiO ₂ - C	40Ni/SiO ₂ - C
27.47	Dibenzofuran	168	—	—	—	1.49	—	3.51	3.55	—	—	7.03	18.67
28.51	Fluorene	166	42.01	51.09	4.51	—	5.23	5.59	7.45	136.38	58.48	15.03	37.16
29.28	1,3-diphenylpropane	196	—	—	1.36	—	—	—	—	—	—	—	2.83
31.06	Phenanthrene	178	83.82	41.83	3.81	10.90	26.95	19.30	18.06	144.76	71.40	10.44	—
31.97	<i>o</i> -Terphenyl	230	1.46	0.66	1.46	0.89	0.74	0.61	0.63	2.32	1.59	1.55	2.69
34.17	Fluoranthene	202	24.26	5.54	2.78	5.56	2.75	2.49	2.01	11.12	9.54	2.94	8.08
34.48	Pyrene	202	32.77	23.09	3.16	7.80	13.62	3.94	2.78	24.20	12.78	2.89	28.86
34.62	<i>m</i> -Terphenyl	230	3.47	2.12	2.49	2.13	1.88	1.14	1.09	4.80	3.18	2.58	5.92
41.98	1,3,5-triphenylbenzene	306	2.44	2.47	2.13	1.55	1.15	—	—	2.90	—	—	3.28
Tar Concentration ($\mu\text{g}_{\text{tar}}/\text{g}_{\text{RDF}}$)			1660.78	775.74	241.00	250.30	577.81	267.98	534.26	1673.16	1095.55	600.72	979.91
Tar Concentration ($\text{mg}_{\text{tar}}/\text{g}_{\text{RDF}}$)			1.66	0.78	0.24	0.25	0.58	0.27	0.53	1.67	1.10	0.60	0.98

Table 4. Classification of tar compounds identified by GC/MS/MS

CLASS 2	CLASS 3	CLASS 4	CLASS 5
Heterocyclic Aromatics	Aromatics 1-Ring	Light PAH 2-3 Rings	Heavy PAH 4-7 Rings
Tars containing hetero atoms; highly water soluble compounds	Light hydrocarbons; do not pose a problem regarding condensability and solubility	Compounds that condense at low temperature even at very low concentration	Components that condense at high temperatures at low concentrations
Furfural	Ethylbenzene	Naphthalene	Fluoranthene
Phenol	p-Xylene	2-Methylnaphthalene	Pyrene
o-Cresol	m-Xylene	Biphenyl	1,3,5-
p-Cresol	o-Xylene	2-ethylpaphthalene	Triphenylbenzene
m-Cresol	Styrene	1-ethylpaphthalene	
2-Methylbenzofuran	Para-methyl Styrene	2,6-dimethylnaphthalene	
Cyclopentanone		1,4-dimethylnaphthalene	
Acetophenone		Fluorene	
2-ethylphenol		1,3-diphenylpropane	
2,4-dimethylphenol		Phenanthrene	
4-ethylphenol		o-Terphenyl	
3-ethylphenol		m-Terphenyl	
2,6-dimethylphenol		Indane	
4-isopropylphenol		Indene	
Dibenzofuran			

Figure Captions

Figure 1. Schematic two-stage pyrolysis-reforming reaction system

Figure 2. BET adsorption-desorption isotherms of fresh catalysts

Figure 3. Tar classification and concentration

Figure 4. DTG-TPO and TGA-TPO of used Ni/SiO₂ catalysts: (a) Sol-Gel, (b) Al, Mg, Ce Sol-Gel, (c) Impregnation.

Figure 5. SEM images, carbon deposition over used Ni/SiO₂ catalysts.

Figure 1. Schematic two-stage pyrolysis-reforming reaction system

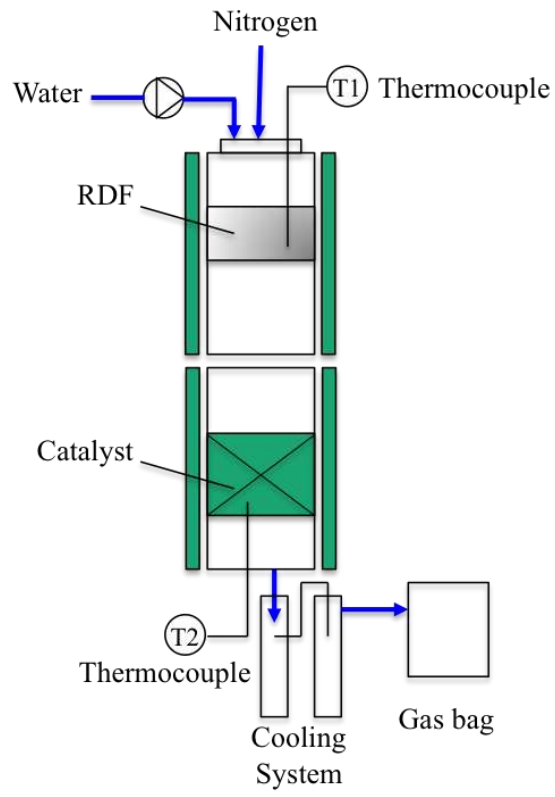
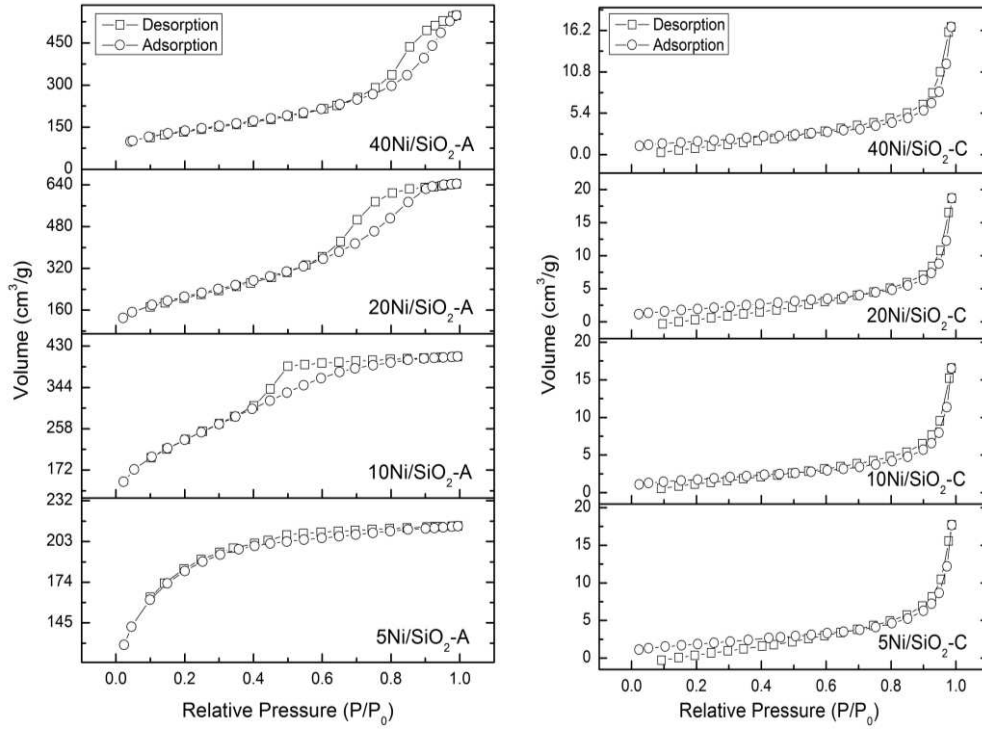
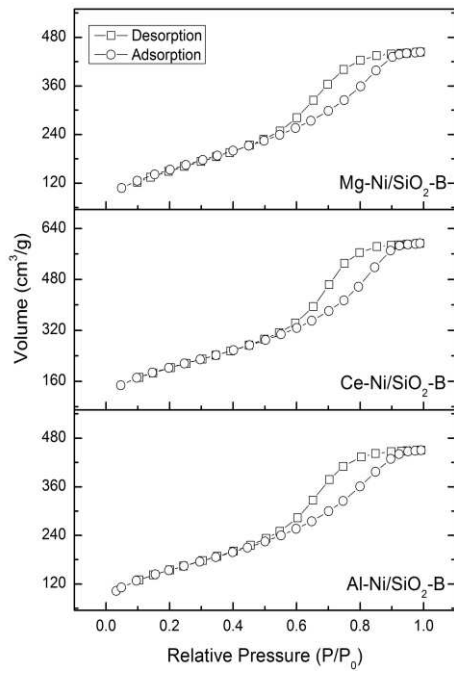


Figure 2. BET adsorption-desorption isotherms of fresh catalysts



(a) 5-40wt% Ni/SiO₂ Sol-Gel

(b) 5-40wt% Ni/SiO₂ Impregnation



(c) 20wt% Ni/SiO₂ Ce, Al, Mg

Figure 3. Tar classification and concentration

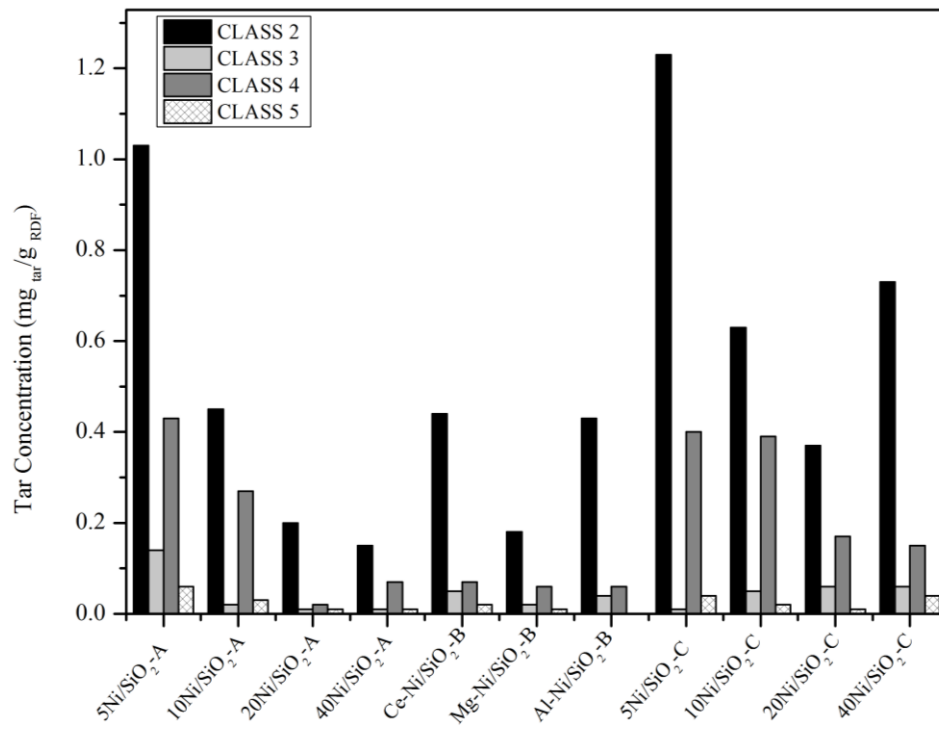
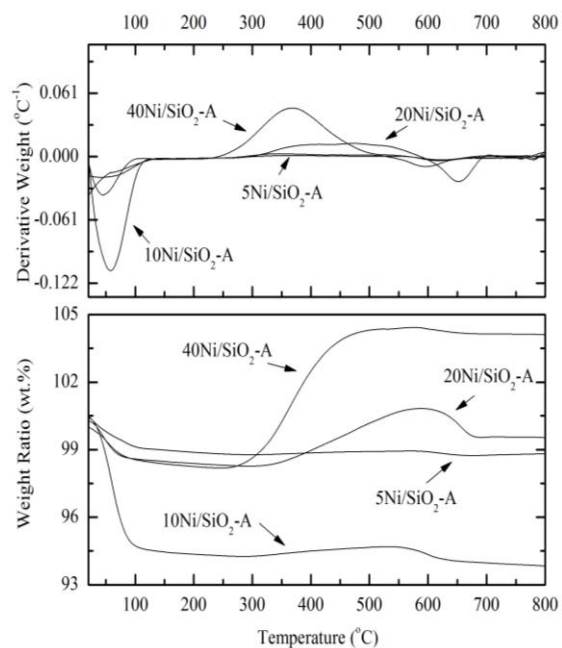
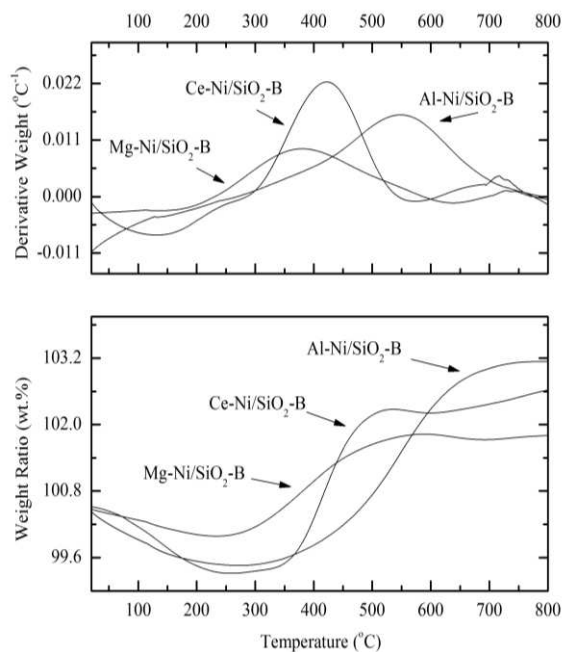


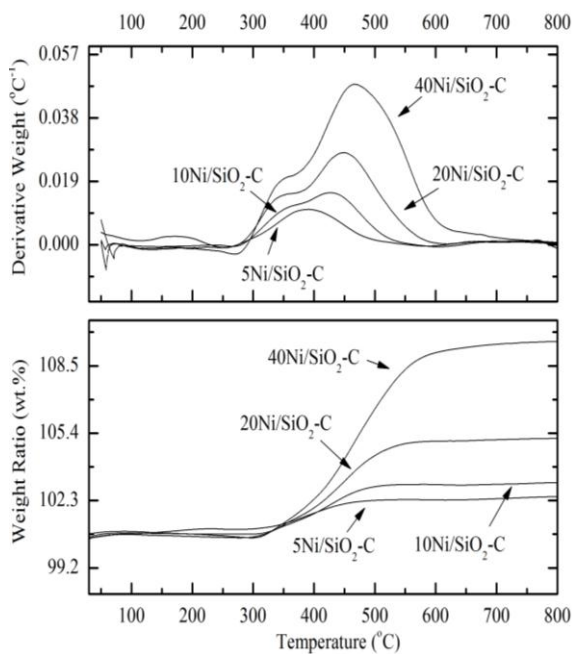
Figure 4. DTG-TPO and TGA-TPO of used Ni/SiO₂ catalysts: (a) Sol-Gel, (b) Al, Mg, Ce Sol-Gel, (c) Impregnation.



a) DTG-TPO, TGA-TPO
5-40wt.% Ni/SiO₂ Sol-Gel

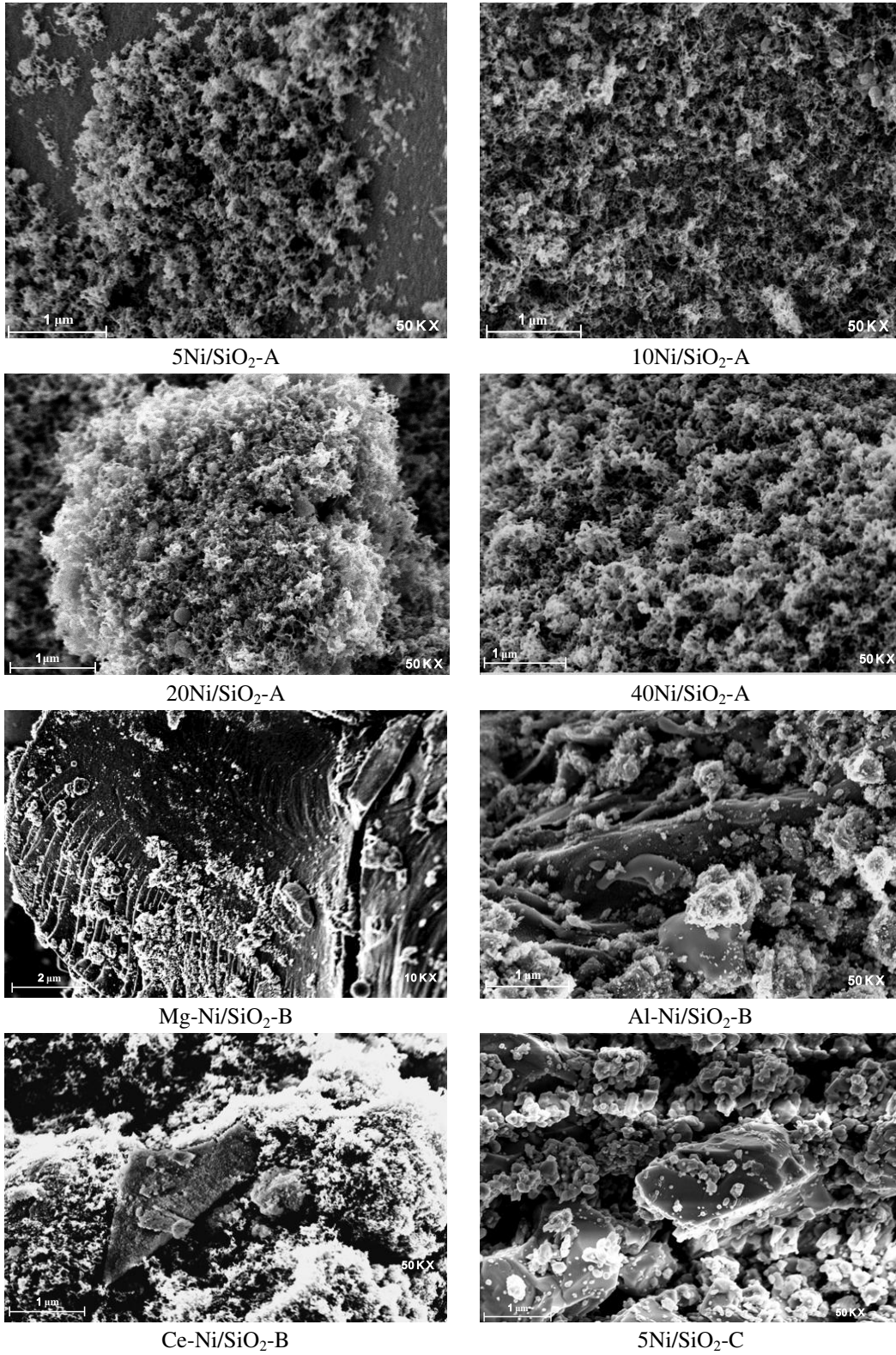


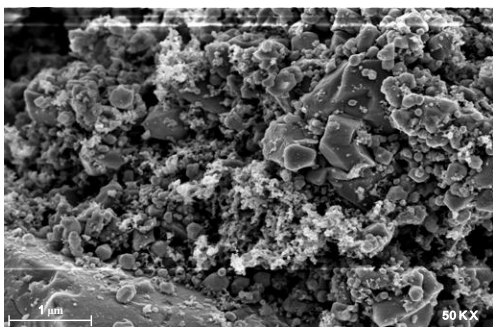
b) DTG-TPO, TGA-TPO Al- Ni/SiO₂, Mg-
Ni/SiO₂, Ce-Ni/SiO₂



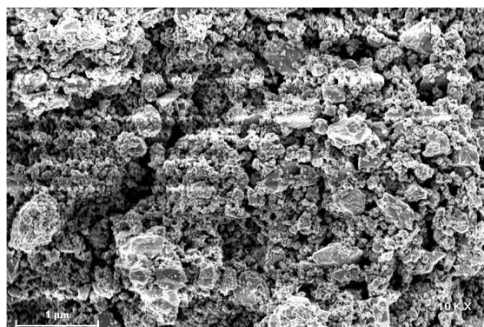
c) DTG-TPO, TGA-TPO
5-40wt.% Ni/SiO₂ Impregnation

Figure 5. SEM images, carbon deposition over used Ni/SiO₂ catalysts.

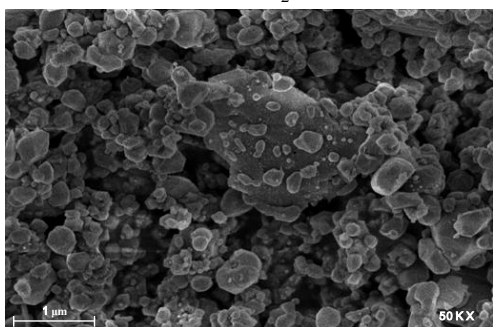




10Ni/SiO₂-C



20Ni/SiO₂-C



40Ni/SiO₂-C